Buckminsterfullerene dihydride, $C_{60}H_2$, has been synthesized, isolated in pure form, and characterized as the 1a1b isomer. As the simplest hydrocarbon derivative of C_{60}, this molecule provides fundamental information regarding the structure of C_{60} derivatives. The results are entirely consistent with the thermodynamic isomer predicted from semiempirical calculations on the 23 possible $C_{60}H_2$ isomers. The presumed borane intermediate, $C_{60}(H)BH_2$, may provide a route to further functionalization of C_{60} and, in a similar fashion, higher fullerenes.

REFERENCES AND NOTES

1. W. Kratschmer, L. D. Lamb, K. Fostiropoulos, D. R. Huffman, *Nature* **347**, 354 (1990).
2. K. M. Creegan *et al.*, *J. Am. Chem. Soc.* **114**, 1103 (1992); Y. Elemes *et al.*, *Angew. Chem. Int. Ed. Engl.* **31**, 351 (1992).
3. T. Suzuki, Q. Li, K. C. Khemani, F. Wudl, O. Almarsson, *Science* **254**, 1186 (1991).
4. J. M. Hawkins, *Acc. Chem. Res.* **25**, 150 (1992).
5. P. R. Birkett, P. B. Hitchcock, H. W. Kroto, R. Taylor, D. R. M. Walton, *Nature* **357**, 479 (1992); F. N. Tebbe *et al.*, *Science* **256**, 822 (1992).
6. R. S. Koefod, M. F. Hudgens, J. R. Shapley, *J. Am. Chem. Soc.* **113**, 8957 (1991).
7. P. J. Fagan, J. C. Calabrese, B. Malone, *Acc. Chem. Res.* **25**, 134 (1992).
8. C. C. Henderson and P. A. Cahill, *Chem. Phys. Lett.* **198**, 570 (1992). A similar study was completed by another group: N. Matsuzawa, D. A. Dixon, T. Fukunaga, *J. Phys. Chem.* **96**, 7594 (1992).
9. C. C. Henderson, C. M. Rohlfing, P. A. Cahill, in preparation. A similar study has been completed by another group: H. R. Karfunkel and A. Hirsch, *Angew. Chem. Int. Ed. Engl.* **31**, 1468 (1992).
10. R. E. Haufler *et al.*, *J. Phys. Chem.* **94**, 8634 (1990).
11. J. March, *Advanced Organic Chemistry* (Wiley, New York, ed. 4, 1992).
12. C. J. Welch and W. H. Pirkle, *J. Chromatog.* **609**, 89 (1992).
13. Semiempirical calculations of a few isomers suggested that this isomer has the lowest heat of formation. The 200-MHz ^1H NMR spectrum of this compound shows an AB quartet centered at δ 5.35 ppm and $^3J_{HH}$ = 14.2 Hz, consistent with nonequivalent, vicinal hydrogenation. Such a product may result from subsequent air oxidation of $C_{60}H_2$ or from reduction of the small amount of $C_{60}O$ present in the reaction mixture. The nomenclature used here may also be used to denote fulleroid substitution patterns, such as C_{60}-1a,1b-diphenylfulleroid, which results from formal diphenylcarbene addition to a 6,6 ring fusion.
14. P. E. Hansen, in *Progress in Nuclear Magnetic Resonance Spectroscopy*, J. W. Emsley, J. Feeney, L. H. Sutcliffe, Eds. (Pergamon, Oxford, 1988), pp. 207–255.
15. A reviewer pointed out that observation of ^{13}C satellites in the ^1H NMR spectrum could be used to rule out a simultaneous intramolecular jump of both hydrogens to another C–C bond. The intensity of such satellites is at the limit of our signal-to-noise ratio because of the low solubility of $C_{60}H_2$. Work with 10% ^{13}C-labeled C_{60} is in progress and should allow us to address this point and to compute carbon hybridizations based on coupling constants.
16. The remote possibility exists that the observed product is the 1a2a (6,5 ring fusion) isomer. This alternate conclusion would represent addition of H_2 across a formal single bond in C_{60}. If it were the thermodynamic product, this would be a failure of both ab initio and semiempirical computational approaches. An x-ray crystal structure may provide conclusive evidence.

17. We thank F. Wudl, C. Yonnani, R. Taylor, E. Kosower, R. M. Milberg, S. Mullen, C. Rohlfing, R. Assink, and D. Wheeler for helpful discussions. Work at Sandia National Laboratories was supported by the U.S. Department of Energy under contract DE-AC04-76DP00789.

21 December 1992; accepted 11 February 1993

Fabrication and Properties of Free-Standing C_{60} Membranes

C. B. Eom, A. F. Hebard, L. E. Trimble, G. K. Celler, R. C. Haddon

Van der Waals forces that bind C_{60} molecular solids are found to be sufficiently strong to allow the reproducible fabrication of free-standing C_{60} membranes on (100) silicon wafers. Membranes, 2000 to 6000 angstroms thick, were fabricated by a modified silicon micromachining process and were found to be smooth, flat, and mechanically robust. An important aspect of the silicon-compatible fabrication procedure is the demonstration that C_{60} films can be uniformly and nondestructively thinned in a CF_4 plasma. Young's modulus and fracture strength measurements were made on membranes with areas larger than 6 millimeters by 6 millimeters. It may be possible to use C_{60} membranes for physical property measurements and applications.

The description of a simple technique to produce macroscopic amounts of C_{60} molecules (*1*) has stimulated numerous investigations into how these molecules can be assembled into solid forms. Crystals (*1–3*) and films (*1, 4*), for example, have been obtained by the sublimation of pure C_{60} at controlled temperatures. These insulating molecular solids have a spherical, close-packed, face-centered-cubic (fcc) structure with a lattice constant of 14.1 Å (*2*) and van der Waals bonding between the molecules. There is ample space in the crystal structure (26% open volume for close-packed spheres) to accommodate guest atoms that, by donating electrons into the C_{60} molecular bands, can induce conducting (*5*) or superconducting (*6*) behavior. In addition, each molecule has degrees of freedom that allow the molecules to tumble independently at gigahertz rates at room temperature (*7, 8*). These remarkable properties alone provide ample motivation to consider novel ways to form and process C_{60} solids.

AT&T Bell Laboratories, Murray Hill, NJ 07974.

In this report, we describe the fabrication and characterization of free-standing C_{60} membranes supported at the edges by (100) oriented Si frames. Membranes have been made with thicknesses in the range 2000 to 6000 Å and areas larger than 6 mm by 6 mm. At first sight, it is remarkable that a van der Waals molecular solid, in which all the molecules are independently rotating at room temperature, should be robust enough to hold together as a free-standing membrane. An estimate of the magnitude of the cohesive forces can be obtained from the heat of sublimation found with the Knudsen technique, 1.65 eV per C_{60} (*9*). The density of molecular bonds for close-packed C_{60} molecules with a nearest-neighbor separation of 10 Å on the (111) plane of the fcc lattice is 1.16×10^{14} cm^{-2}, which, if we ignore near-neighbor correlation effects, at 1.65 eV for each C_{60}–C_{60} bond, gives an energy density of 310 ergs/cm^2. If we assume that this energy falls to zero when the surfaces are separated by, say, a molecular diameter (10 Å), then the specific cohesive force can be calculated as (310 ergs/cm)/1.0×10^{-7} cm = 3.1×10^9 dynes/cm^2. Typical van der Waals specific adhesion forces for chemically inert films are approximately 10^9 dynes/cm^2 (*10*). Thus, in a very approximate comparison, it is not unreasonable to expect that these forces, which are sufficiently strong to give rise to robust adhesion, should likewise be strong enough to give robust cohesion in a free-standing membrane. The observation that C_{60} films on substrates such as glass survive the Scotch Tape adhesion test (*4*) supports this line of reasoning.

In this report, we describe our fabrication procedure, which makes good use of conventional Si processing techniques. An important component of this procedure is the use of a CF_4 plasma to remove a Si_3N_4 etch-stop layer without damaging the C_{60} film. Then we demonstrate that such plasmas can also be used to uniformly thin a C_{60} film without damaging the remaining film. Characterization of the membranes by x-rays and bulge testing provides information about the structure and mechanical properties such as Young's modulus, internal stress, and fracture strength. We conclude with a discussion of how these membranes might be used in investigations of physical properties or in applications such as gas atom or ion filters and masks for x-ray lithography.

Figure 1 shows schematically the processing steps used in fabricating the C_{60} membranes. This process is adapted from typical Si micromachining techniques (*11*). First, low-stress Si_3N_4 films 1000 Å thick are deposited on both sides of (100) Si wafers that are 2 inches in diameter and 100 μm thick. Conventional photolithography is then used to make features on the wafer. The final feature size depends on the wafer thickness and can be calculated by considering the anisotropic etching angle (~54°). The edges of the rectangular features are aligned along the [011] in-plane orientation of the Si wafer. We remove the Si_3N_4 on the features by using a CF_4 plasma generated in a reactive ion beam etching system. The CF_4 gas flow rate and total pressure are 10 standard cubic centimeters per minute and 10 mtorr, respectively. The radio-frequency power on the diode (70 W) generates a self-bias voltage of 200 V.

After the Si_3N_4 has been removed, the wafer is etched anisotropically in 6.9 M KOH solution (100 ml of water + 44 g of KOH) at 70°C. Under these conditions the etch rate of Si along the [100] direction is approximately 1 μm/min. After etching, the Si_3N_4 membrane remains because Si_3N_4 is relatively inert to the KOH solution and is strong enough to survive. Subsequent to this step (panel D in Fig. 1), C_{60} films are deposited onto the Si_3N_4 on the opposite side of the Si wafer. The deposition conditions and characteristics of the C_{60} films are discussed elsewhere (*4*). The final and perhaps most critical step is the use of CF_4 plasma etching to remove the Si_3N_4 film adjacent to the C_{60} in the exposed areas of the wafers. The C_{60} etch rate under these conditions is ~150 Å/min, slower by a factor of 2 than the etch rate for Si_3N_4 under the same conditions. This relatively slower etch rate of C_{60} with respect to Si_3N_4 is essential for the fabrication of the C_{60} membranes.

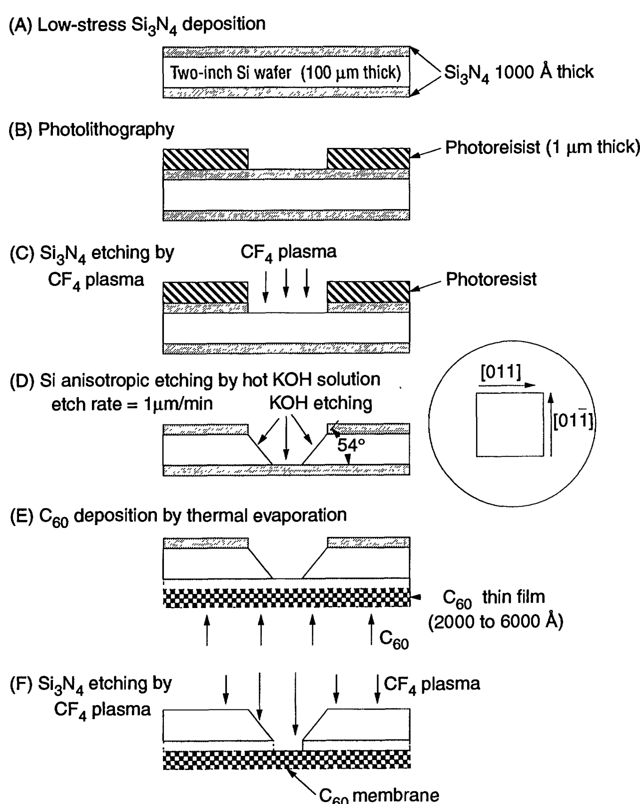

Fig. 1. Sequence of deposition and etching steps used to fabricate C_{60} membranes on (100) oriented Si.

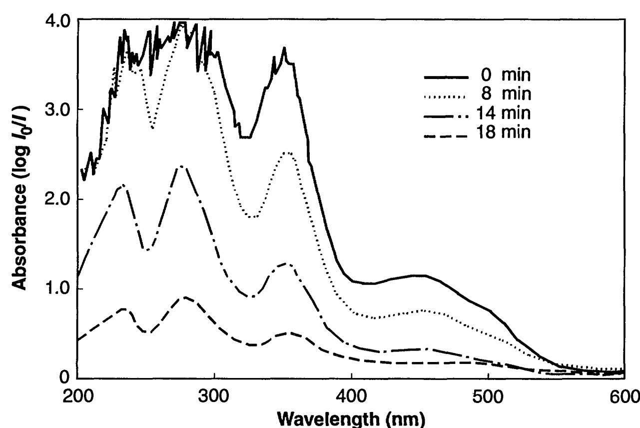

Fig. 2. Dependence of ultraviolet-visible absorbance on wavelength for a C_{60} film, initially 3200 Å thick, deposited onto quartz and plasma etched with CF_4 for the times indicated in the legend.

The slower etch rate of C_{60} as compared to Si_3N_4 or Si in the CF_4 plasma can be explained by different etching mechanisms. When Si or Si_3N_4 is exposed to a CF_4 plasma, etching is facilitated by chemical reactions and the generation of volatile by-products such as SiF_4 (*12*). In contrast, the C_{60} films are etched by a sputtering process (simple momentum transfer), and there is no chemical reaction between C_{60} and the excited species in the CF_4 plasma. We have confirmed this by comparing the etch rate for C_{60} and Si_3N_4 in a CF_4 plasma with the etch rate in an Ar^+ plasma having similar etching parameters. The etch rate for C_{60} in Ar^+ is about 100 Å/min, in contrast to the negligible etch rate for Si_3N_4 and Si. The slower etch rate for C_{60} in the Ar^+ plasma relative to that in the CF_4 plasma is due mainly to the lighter mass of Ar^+ compared to the heavier species in the CF_4 plasma (for example, mass of Ar, 40; CF_2, 50; CF_3, 69; and CF_4, 88).

Because the C_{60} membranes must be exposed to the CF_4 plasma during the last step of the processing, it is important to check for structural damage to the C_{60} caused by exposure to the CF_4 plasma. We did this by monitoring the optical density of a C_{60} film initially 3200 Å thick as a function of etching time. This reference film was deposited onto a quartz substrate, etched for a recorded time, measured ex situ, etched again, and so on. Figure 2 shows absorbance over the wavelength range 200 to 600 nm for the subset of etching times identified in the legend. The absorbance at each of the four prominent peaks in Fig. 2 is displayed in Fig. 3 as a function of etched film thickness (measured with a profilometer). The peak intensities decrease with etching time, but the peak positions remain constant. The measured absorbance is linear in thickness as would be expected for exponential attenuation. The linear extrapolation of the four different absorbances to the same thickness (~3200 Å) where the film is completely removed indicates that the relative peak heights do not change during processing. Accordingly, at all stages of etching, the thinned film has a spectrum that is identical to that of pure C_{60}, and there is negligible damage to the C_{60} during processing. The absorbance is sensitive to C_{60} molecular damage caused by the etching CF_4 ions but

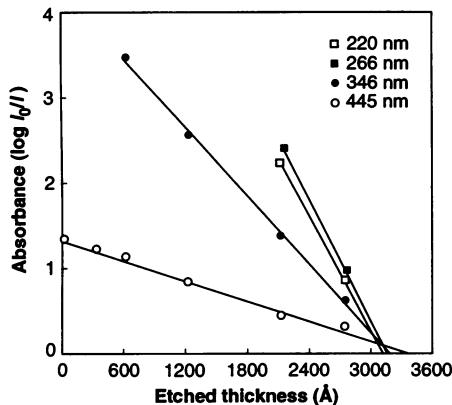

Fig. 3. Absorbance at the peak wavelengths of Fig. 2 (identified in the legend) versus measured etched film thickness. The linear dependences and their convergence to a thickness near the starting thickness of 3200 Å indicates that the C_{60} film is uniformly thinned without damage to the remaining film.

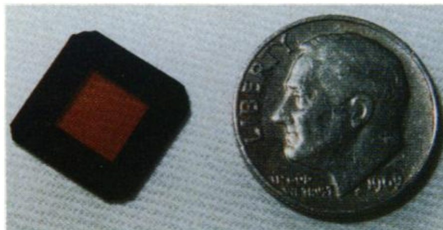

Fig. 4. Photograph of a free-standing C_{60} membrane 5730 Å thick with an area of 6.4 by 6.4 mm^2.

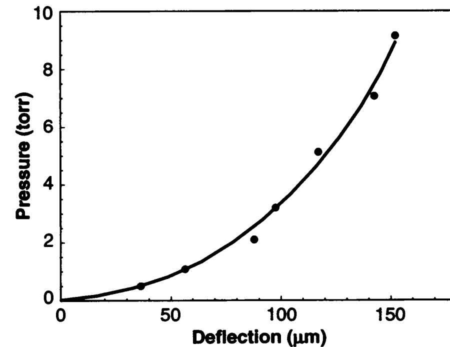

Fig. 5. Differential pressure across a 3860 Å thick C_{60} membrane versus deflection. The analysis of elastic properties is discussed in the text.

not to structural changes in the fcc lattice, which might be present near the surface of the etched film.

The photograph in Fig. 4 shows a finished membrane in reflected light. The film is 5730 Å thick, and the area is 6.4 by 6.4 mm^2. The prominent yellow color is characteristic of C_{60} films sublimed onto transparent substrates (*1, 4*).

We determined the mechanical properties of two separate C_{60} membranes by applying a differential pressure P to the membrane and monitoring the displacement h of the membrane center. The tensile stress σ_0, Young's modulus E, and Poisson's ratio ν are related to these measured quantities by the equation (*13, 14*)

$$P = \frac{12th}{a^2}\left[\sigma_0 + \frac{1.8Eh^2}{(1-\nu)a^2}\right] \quad (1)$$

where a and t are the membrane side length and thickness, respectively. Shown in Fig. 5 is a plot of P versus h for a square membrane that is 3860 Å thick and 6.4 mm on a side. The data for several deflection cycles overlap well, indicating elastic rather than plastic behavior. The solid-line regression fit of Eq. 1 to the data gives $\sigma_0 = 12.7$ MPa for the tensile residual stress and $E/(1 - \nu) = 55.4$ GPa for the effective modulus. Results for a second membrane, 3440 Å thick, were $\sigma_0 = 21.2$ MPa and $E/(1 - \nu) = 99.6$ GPa. For comparison, the corresponding values of $E/(1 - \nu)$ for diamond and glassy C (GC20) are 1172 and 38.5 GPa, respectively (*15*). A value for Young's modulus of $E = 15.9$ GPa for solvated C_{60} crystals has been measured in a vibrating reed experiment (*16*). Although this value cannot be directly compared with our result because of the unknown Poisson ratio ν, one might expect the presence of solvent residues in the single crystals to give degraded elastic properties. The factor of ~2 difference between the elastic constants of the two membranes reported here may be the result of processing variations and the use of different thickness substrates. Both membranes fractured near a differential pressure of 10 torr, corresponding roughly to fracture strengths in the range 75 to 95 MPa. For polycrystalline Si membranes in the same apparatus, the fracture strength can exceed 1 GPa (*17*).

X-ray examination of a C_{60} membrane 5730 Å thick in both transmission and reflection revealed an fcc structure with randomly oriented grains ~60 Å in size. The x-ray spectrum is essentially the same as that of C_{60} films similarly prepared on quartz substrates (*4*). There are differences, however, in the intrinsic stresses of membranes of different thicknesses. The as-prepared thinner membranes (~2000 Å) are usually wrinkled. These wrinkles can be removed by vacuum annealing at 300° to 400°C and then cooling to room temperature. The as-prepared thicker membranes (~6000 Å) are always taut and remain so under vacuum annealing conditions. Upon cooling after the anneal, however, the additional tension introduced by the annealing that was responsible for removing the wrinkles in the thinner films will, in the thicker films, occasionally cause membrane rupture. Because the thermal expansion coefficient of 2×10^{-5} K^{-1} is rather high (*18*), a temperature change of 100°C can introduce critical stresses. Relaxation effects that might mediate these stresses are presently not understood. Further work is needed to ascertain whether thicker membranes (≳6000 Å) can be fabricated with larger (≳1 cm) areas. We expect that membranes less than 1000 Å thick are possible with areas less than 1 mm^2.

Having demonstrated that reasonably robust C_{60} membranes can be reproducibly fabricated, it is worthwhile to comment on how they might be used. Free-standing membranes are advantageous for physical characterization studies where the absence of a substrate greatly facilitates the measurement [such as electron energy loss, infrared absorption, and transmission electron microscopy (TEM)]. Similar considerations hold in experiments in which C_{60} is doped from the vapor phase by alkali metals. There is no worry about diffusion into and interaction with an underlying substrate, and the Si support frame can be advantageously used as a mask.

Because carbon with its six electrons has a low cross section to x-rays and high-energy electrons, C_{60} membranes might be considered as "transparent" substrates for TEM sample preparation and as masks in x-ray lithography. A unique advantage of the C_{60} solid in such applications is its smooth surface and its low density of 1.67 g/cm^3, a factor of 2 lower than diamond and 0.73 times that of graphite. X-ray lithography masks require mechanical stiffness to maintain dimensional stability, so it would be necessary to improve the mechanical properties of the present membranes. Polycrystalline Si, which is considered a good candidate for x-ray masks (*17*), has $E/(1 - \nu)$ a factor of 3 higher than the C_{60} membrane measured in Fig. 5. However, in the soft x-ray region near the C_K absorption edge at 284 eV (43.6 Å), C_{60} membranes would be significantly more transparent than Si. A possible application at these wavelengths might be in projection x-ray lithography (*19*).

Finally, one might think of a free-standing C_{60} membrane as the quintessential micropore filter. The membrane should be permeable to some gases and not to others. It is known, for example, that, under pressure, significant amounts of hydrogen compared to oxygen can be stored in crystalline material (*20*). Also, variability in the mobility of particular ionic or atomic species might be useful in sensor applications where selectivity is desired.

REFERENCES AND NOTES

1. W. Krätschmer, L. D. Lamb, K. Fostiropoulos, D. R. Huffman, *Nature* **347**, 354 (1990).
2. R. M. Fleming *et al.*, *Mater. Res. Soc. Symp. Proc.* **206**, 691 (1991).

3. R. L. Meng *et al.*, *Appl. Phys. Lett.* **59**, 3402 (1991).
4. A. F. Hebard, R. C. Haddon, R. M. Fleming, A. R. Kortan, *ibid.*, p. 2109.
5. R. C. Haddon *et al.*, *Nature* **350**, 320 (1991).
6. A. F. Hebard *et al.*, *ibid.*, p. 600.
7. C. S. Yannoni *et al.*, *J. Phys. Chem.* **95**, 9 (1991).
8. R. Tycko *et al.*, *ibid.*, p. 518.
9. J. Abrefah, D. R. Olander, M. Balooch, M. Siekhaus, *Appl. Phys. Lett.* **60**, 1313 (1992).
10. M. Ohring, *The Materials Science of Thin Films* (Academic Press, New York, 1992), p. 442.
11. K. E. Petersen, *Proc. IEEE* **70**, 420 (1982).
12. T. Sugano, *Applications of Plasma Processes to VSLI Technology* (Wiley, New York, 1985), p. 43.
13. J. W. Beams, in *Structure and Properties of Thin Films*, C. A. Neugebauer, J. B. Newkirk, D. A. Vermilyea, Eds. (Wiley, New York, 1959), pp. 183–192.
14. J. A. Walker, K. J. Gabriel, M. Mehregany, in *Proceedings of the IEEE Micro-Electro Mechanics Systems Workshop*, Napa Valley, CA, February 1990 (IEEE, New York, 1990), pp. 56–65.
15. J. Robertson, *Phys. Rev. Lett.* **68**, 220 (1992).
16. X. D. Shi *et al.*, *ibid.*, p. 827.
17. L. E. Trimble and G. K. Celler, *J. Vac. Sci. Technol. B* **7**, 1675 (1989).
18. P. A. Heiney *et al.*, *Phys. Rev. B* **45**, 4544 (1992).
19. J. E. Bjorkholm *et al.*, *J. Vac. Sci. Technol. B* **8**, 1509 (1990).
20. R. A. Assink *et al.*, *J. Mater. Res.* **7**, 2136 (1992).

21. We thank R. M. Fleming for x-ray characterization, T. A. Fulton for assistance with mask generation, and R. H. Eick and J. H. Marshall for technical assistance. We also appreciate useful discussions with J. M. Phillips.

26 October 1992; accepted 31 December 1992

Outgassed Water on Mars: Constraints from Melt Inclusions in SNC Meteorites

Harry Y. McSween, Jr.,* and Ralph P. Harvey

The SNC (shergottite-nakhlite-chassignite) meteorites, thought to be igneous rocks from Mars, contain melt inclusions trapped at depth in early-formed crystals. Determination of the pre-eruptive water contents of SNC parental magmas from calculations of the solidification histories of these amphibole-bearing inclusions indicates that martian magmas commonly contained 1.4 percent water by weight. When combined with an estimate of the volume of igneous materials on Mars, this information suggests that the total amount of water outgassed since 3.9 billion years ago corresponds to global depths on the order of 200 meters. This value is significantly higher than previous geochemical estimates but lower than estimates based on erosion by floods. These results imply a wetter Mars interior than has been previously thought and support suggestions of significant outgassing before formation of a stable crust or heterogeneous accretion of a veneer of cometary matter.

Torrents of running water have scoured the ancient, heavily cratered crust of Mars to produce valley networks, and a variety of more recent features (softened terrain, pedestal craters, patterned ground) testify to the presence of subsurface water or ice (*1*). Under present atmospheric conditions, however, liquid water is unstable everywhere on the planet's surface, water ice is stable on the surface only at the poles, and only minute amounts of water vapor are present in the martian atmosphere. Although ice at the polar caps may be equivalent to a global average water depth of perhaps 20 m (*2*), most of the planet's water is probably hidden from view as permafrost or ground water. As much as 1000 m of globally distributed water could be stored within the upper 10 km of the crust (*3*). Because most of the water on Mars cannot be imaged by spacecraft, it is difficult to quantify the amount of water that has been outgassed.

One estimate of outgassed water, extrapolated from the amount of erosion caused by a large flood in the Chryse basin, corresponds to global depths of >440 m (*2*). This is a minimum estimate, because it was assumed that water carried its maximum sediment load. Even larger amounts of water are required by the proposed former existence of martian seas (*4*). (For comparison, Earth has outgassed enough water to cover its surface uniformily to a depth of 2700 m.)

A contrary view is provided by measurements of the total volume of igneous materials on Mars, which are the source of its outgassed water. A recent estimate, based on the assumption that martian magmas have water contents similar to those of typical terrestrial basaltic magmas (1% by weight), corresponds to a global water depth of 150 m (*5*).

Other, independent estimates are based on the composition of the martian atmosphere. Atmospheric hydrogen, nitrogen, and argon isotopic abundances suggest that the amounts of outgassed water were limited, corresponding to global depths of 3.6, 8 to 133, and 6 to 10 m, respectively (*6*). Atmospheric carbon and oxygen isotopic compositions are consistent with an outgassed water depth of perhaps 50 to 60 m (*7*). These values, however, rest on questionable assumptions that impact erosion of the atmosphere has been negligible, that ratios of noble to other gases were uniform among the terrestrial planets and remained unchanged during hydrodynamic escape, that escape rates for CO_2 and H_2O over time are adequately estimated, that climatic conditions in the past were similar to those of the present, and other complications (*8*).

The SNC meteorites are believed to be martian igneous rocks ejected during large impacts (*9*). Another estimate for the amount of outgassed water is based on a model for the bulk composition of the SNC meteorite parent body formulated from element ratios in the meteorites. Calculations of the original volatile inventory of this parent body suggest that it was significantly enriched in volatile elements and water relative to Earth, but the model assumes that most of its water was lost through reaction with metallic iron during core formation early in the planet's history (*10*). The water content of the martian mantle, calculated from ratios of the abundance of water to the abundances of other volatile species in bulk SNC meteorites and its solubility in magmas, is only 36 ppm (*11*). If all of this water were outgassed, it would form a global ocean 130 m deep. However, more reasonable degrees of outgassing imply that the amount of water was smaller, perhaps 10 to 20 m. This estimate depends critically on the assumption of homogeneous accretion by which Mars lost its original water through planet-wide equilibration, an accretion model different from that advocated for Earth.

These conflicting estimates for martian outgassed water can be reconciled in several ways: The measured volume of igneous materials presumably represents volcanic activity since 3.9 billion years ago, the time at which stable crust began to form. Any magmatism and outgassing before that time left no rock record, so this represents a minimum estimate. The addition of non-outgassed water through late accretion of a veneer of cometary material (*12*) could also explain the discrepancy between estimates based on igneous materials and those based on erosion by floods. The SNC parent body model can be reconciled with other water estimates if the need for homogeneous accretion is relaxed, so that not all water is lost through reaction with metallic iron. The lower atmospheric estimates can be understood if Mars lost part of its early atmosphere by impact erosion or hydrodynamic escape.

The estimate of martian outgassing based on the volume of volcanic materials represents a critical lower limit for the planet's water inventory, one that can be quantified further by a consideration of

Department of Geological Sciences, University of Tennessee, Knoxville, TN 37996.

*To whom correspondence should be addressed.